PHYSICAL REVIEW B VOLUME 24, NUMBER 9 1 NOVEMBER 1981

Simple three-state model with infinitely many phases

David A. Huse
Laboratory of Atomic and Solid State Physics, Cornell University, Ithaca, New York 14853
(Received 23 March 1981)

A nearest-neighbor three-state model is introduced that has chiral interactions and exhibits spatially modulated order. A Migdal-Kadanoff renormalization group for this model is constructed and analyzed for general dimensionality d. This renormalization group is exact when applied to the model on certain hierarchical or fractal lattices. The resulting phase diagrams are of remarkable complexity: They exhibit an infinite number of distinct ordered phases, each identified by q, the principle wave number of the modulations in the local order. All ordered phases are commensurate with the lattice structure, and for sufficiently large d there is apparently a phase for every rational fraction q.

I. INTRODUCTION

Recently considerable attention has been addressed to simple theoretical models that exhibit, or appear to exhibit, spatially modulated ordered phases.[1–7] Particularly interesting, in view of the simplicity of its Hamiltonian and the diversity of its apparent behavior, is the axial next-nearest-neighbor-Ising (or ANNNI) model,[2–6] an Ising model with competing interactions. For spatial dimensionality $d > 2$ this model has been shown, at low temperatures, to have an infinite number of distinct ordered phases, each phase being distinguished by a wave number characterizing the spatial modulations in the local order.[5]

In this paper we discuss a class of p-state models ($p = 2, 3, \ldots$) with only nearest-neighbor (noncompeting) interactions that are a generalization of the Potts models[8] and of the discrete planar or clock models.[9] It is first pointed out that the ANNNI model can be regarded as a four-state model with nearest-neighbor but reflection noninvariant (or chiral) interactions and spatial anisotropy. Viewed from this perspective the ANNNI model is not quite the simplest system that might be expected to exhibit modulated order with variable wave number. In fact, it appears that the simplest p-state model with only nearest-neighbor, noncompeting interactions to exhibit such spatially modulated correlations is the three-state chiral model introduced below. Recently Ostlund[7] has independently studied this model in two dimensions with spatially anisotropic interactions in the context of the commensurate-incommensurate phase transition.

The major part of the present paper is devoted to the three-state chiral model. To gain orientation, the general solution for a one-dimensional lattice and a corresponding exact decimation or dedecoration renormalization group[10] are presented in Sec. III. The full sixfold symmetry of the three-state chiral model on any d-dimensional layered lattice is then established in Sec. IV. The correlation functions are thence shown to exhibit well-defined spatial modulations under appropriate conditions. Section V introduces a Migdal-Kadanoff renormalization-group scheme[11,12] for the three-state chiral model. This is approximate for a d-dimensional hypercubic lattice, with $d > 1$, but is *exact* when applied to the model on certain pseudolattices or fractal lattices of a hierarchical nature[13–16] (see Fig. 3 below). Sections VI and VII discuss the phase diagrams predicted by the renormalization-group analysis. By means of the renormalization group the wave number q describing the modulations in the local order is readily identified for all ordered phases.

The phase diagrams of the three-state chiral model resulting from the Migdal-Kadanoff renormalization group, and their evolution as d is increased prove to be surprisingly rich in detail, with infinitely many phases appearing at various borderline dimensions. Of course it must be recognized that our renormalization-group analysis is only approximate as applied to the model on a realistic two- or three-dimensional lattice so the results may not be *physically* relevant. Some of the details discovered are clearly artifacts of the particular renormalization-group scheme adopted. For example, the main or "principal" phases are all found to have wave numbers of the form $q = m/3(2^n)$ with m and n integral. The factor 2^n in the denominator here is a result of the adoption of a renormalization-group scheme that rescales the lattice by a factor of $b = 2$ at each stage. Thus, as is generally true for simple Migdal-Kadanoff renormalization groups, only the more qualitative features of the results should be taken seriously as possibly applying to realistic situations. Nevertheless, the complex results we find do represent an *exact* solution to a well-defined statistical problem, namely, the three-state chiral model on a class of hierarchical lattice

structures. Although these structures are rather artificial, containing sites of indefinitely high coordination number, the details of the results do have a definite interest in the context of these systems and, we also believe, the general features may have wider validity.

In fact, we find an ordered phase with modulations in the local order characterized by a wave number q for every rational fraction in the first Brillouin zone (which is described by $0 \leq q < 1$ in our convention: see below). Each such phase is present only for dimensionalities greater than or equal to a borderline dimension, $d^*(q)$, at which the phase first appears. The simplest ordered phases, with $q = 0$, $\frac{1}{3}$, or $\frac{2}{3}$, are all equivalent under the symmetries of the model to the ordered phase of the ferromagnetic Potts model and are therefore present for all $d > d^*(0) = 1$. The next group of ordered phases do not appear until two dimensions ($d = 2$), but for $d > 2$ the phase diagram rapidly fills in with many further new phases, apparently completing the process after the appearance of infinitely many families of infinitely many phases at an ultimate borderline dimension, $d_f = d^*(\frac{1}{9}) \simeq 2.625$, with the appearance of the $q = \frac{1}{9}$ ordered phase. A relatively few ordered phases, namely, those with $q = m2^{-n}/3$ where n is small, occupy significant areas in the phase diagram. For $d \gtrsim 2.5$ there are regions in the phase diagram between these principal phases that contain many distinct ordered phases, each occupying an extremely slender region and all with very large correlation lengths. A calculation or experiment of finite resolution would probably be able to resolve only a finite number of ordered phases. Then the wave number characterizing the modulations in the order might appear to vary continuously, giving the appearance of incommensurate order, between the commensurate phases that are resolved.

Because of the simplicity of the model the full phase diagrams and (discrete) renormalization-group flows can all be represented on a plane parametrized by the real and imaginary parts of an appropriate transfer-matrix eigenvalue λ (see Figs. 1 and 2 below). The reader uninterested in the detailed arguments can gain an impression of our results by perusing the figures illustrating the phase diagrams for various dimensionalities (Figs. 4 to 8). In particular, Fig. 10 below shows a representation of the results in a form, exhibiting a unique multiphase point, comparable to the phase diagrams of the ANNNI model.[3–5] Self-similar devil's-staircase behavior[15] of the variation of the wave number q across the phase diagram is illustrated in Fig. 9.

II. ONE-DIMENSIONAL p-STATE MODELS

Consider a homogeneous system of "spins" on a one-dimensional lattice with interactions of strictly finite range. Suppose each spin variable can take on p_0 different values, and the interaction of the longest range is between mth neighbor spins. Such a system is exactly equivalent to a system of spins that can take on $p = p_0^m$ values and have only nearest-neighbor interactions. The correspondence is made by subdividing the chain of p_0-state spins into blocks of m adjacent spins. Each such block of m p_0-state spins interacts only with adjacent blocks and can be considered as a p-state spin, s_i, that can take the values, say, $s_i = 0, 1, 2, \ldots, p-1$. Let us define projection operators P_i^k such that

$$P_i^k = \delta_{k,s_i} = \begin{cases} 1, & \text{if } s_i = k \\ 0, & \text{if } s_i \neq k \end{cases} . \tag{2.1}$$

Then the general Hamiltonian for such a chain of p-state spins is

$$\mathcal{H} = -\sum_i \sum_{k=0}^{p-1} \sum_{l=0}^{p-1} J_{kl} P_i^k P_{i+1}^l . \tag{2.2}$$

The ANNNI model in d dimensions can be thought of as parallel Ising chains making up a hypercubic lattice. The interchain coupling is via ferromagnetic nearest-neighbor bonds. Within each chain, though, there are also antiferromagnetic second-neighbor bonds. The Hamiltonian for a single such chain in isolation is

$$\mathcal{H} = -J\left[\sum_i s_i s_{i+1} - \kappa \sum_i s_i s_{i+2}\right] . \tag{2.3}$$

Though it is not the easiest way to analyze this one-dimensional ANNNI model,[17] a direct mapping can be made onto a four-state model with only nearest-neighbor couplings in the fashion described above. Each block of two Ising spins can assume four different states and interacts only with its nearest-neighbor blocks. The same mapping can be made from the ANNNI model in any dimensionality to a four-state model with nearest-neighbor interactions only, though with spatially anisotropic couplings. There is the possibility that the behavior seen in the ANNNI model may appear in some simpler four-state model, for example with isotropic couplings. The bulk of this paper concentrates on the simplest three-state model that exhibits multiphase behavior similar to that seen in the ANNNI model.[3–5]

For many purposes this mapping of a model with simple spins and longer-range interactions onto a model with only nearest-neighbor interactions between more complicated spins is not very helpful: for two purposes, though, it is useful. First, the Migdal-Kadanoff approximate renormalization group[11,12] depends on bond moving. In a lattice with only nearest-neighbor interactions the procedure is straightforward. Second, in a one-dimensional system the application of transfer matrix techniques is

simplest when there are only nearest-neighbor interactions along the chain.

The $p \times p$ transfer matrix for the linear chain Hamiltonian (2.2) is

$$\underline{T} = [T_{kl}] = [e^{K_{kl}}] \ , \tag{2.4}$$

where $K_{kl} = \beta J_{kl}$. This matrix has p eigenvalues, λ_m, each with right and left eigenvectors, $\vec{e}^{R,m}$ and $\vec{e}^{L,m}$.[18] The eigenvalues are either real or occur in complex conjugate pairs. The largest eigenvalue will be real and positive and we will number the eigenvalues so that $\lambda_0 \geq |\lambda_1| \geq |\lambda_2| \ldots$. The basic pair correlation functions for this system are

$$G^{kl}(n) = \langle P_i^k P_{i+n}^l \rangle \ . \tag{2.5}$$

In the thermodynamic limit these correlation functions may be written in terms of the eigenvalues and eigenvectors of the transfer matrix as

$$G^{kl}(n) = e_k^{L,0} e_l^{R,0} \sum_{m=0}^{p-1} e_k^{R,m} e_l^{L,m} \left(\frac{\lambda_m}{\lambda_0} \right)^n \ , \tag{2.6}$$

when $\lambda_0 > |\lambda_1|$. There are p^2 such real correlation functions which are, in general, independent except for the single restriction

$$\sum_{k=0}^{p-1} \sum_{l=0}^{p-1} G^{kl}(n) = 1 \ . \tag{2.7}$$

Asymptotically, for large spin separation n, the behavior of a correlation function $G(n)$ is dominated by the eigenvalues of greatest magnitude. If λ_1 is real and positive then $G(n)$ is asymptotically monotonic. If λ_1 is real and negative, $G(n)$ will be modulated with a wavelength of two sites, as in the antiferromagnetic Ising chain. If λ_1 and λ_2 are a complex-conjugate pair, the correlations vary as

$$G(n) = G_\infty + G_1 |\lambda_1/\lambda_0|^n \cos(2\pi q n + \phi) + \cdots \ , \tag{2.8}$$

where $\lambda_1 = |\lambda_1| e^{2\pi i q}$. Thus with complex eigenvalues the correlation functions can have modulations of any wavelength.

For the Ising model one has $p = 2$ and the transfer matrix cannot have complex eigenvalues since a 2×2 matrix with non-negative real elements has only real eigenvalues. As shown below, the simplest model with only nearest-neighbor interactions but exhibiting complex eigenvalues is a $p = 3$ system.

Consider then the class of p-state models in which the p-fold cyclic symmetry is not broken. The asymmetric clock models[7] are a subset of this class of models. A physical picture of such a model is that the spin at site i is a unit vector in the xy plane at an angle $\theta_i = 2\pi s_i/p$ from the x axis. The cyclic symmetry is unbroken if the interaction energy between two such spins depends only on the angle between them, namely $(\theta_i - \theta_j) = 2\pi(s_i - s_j)/p$. More precisely, we require that if $k - l = k' - l' \pmod p$ then $J_{kl} = J_{k'l'}$. It follows that the transfer matrix T is cyclic with eigenvalues and eigenvectors

$$\lambda_m = \sum_{k=0}^{p-1} J_{0k} e^{2\pi i m k/p} \tag{2.9}$$

and

$$e_l^{R,m} = [e_l^{L,m}]^* = p^{-1/2} e^{2\pi i m l/p} \ . \tag{2.10}$$

The expression (2.6) then yields the correlation function as

$$G^{kl}(n) = p^{-2} \sum_{m=0}^{p-1} e^{2\pi i (k-l) m/p} \left(\frac{\lambda_m}{\lambda_0} \right)^n \ . \tag{2.11}$$

There are now only p distinct correlation functions, one for each value of $k - l \pmod p$. Thus the restriction (2.7) leaves, in general, $(p-1)$ *independent* real correlation functions.

Alternatively, we may use the complex correlation functions

$$\begin{aligned} G_m(n) &= \langle e^{2\pi i (s_{i+n} - s_i) m/p} \rangle \\ &= \sum_{k=0}^{p-1} \sum_{l=0}^{p-1} e^{2\pi i (l-k) m/p} G^{kl}(n) \\ &= \left(\frac{\lambda_m}{\lambda_0} \right)^n \end{aligned} \tag{2.12}$$

for $m = 1, 2, \ldots, p-1$. From (2.9) we see $G_k(n) = G_{p-k}^*(n)$ so the set of independent correlation functions of this type is $G_m; m = 1, \ldots, [\frac{1}{2}p]$. For p odd the set of $(p-1)$ independent real correlation functions (2.11) can thus be replaced by an equivalent set of $\frac{1}{2}(p-1)$ independent *complex* correlation functions. This is particularly useful for $p = 3$ as all pair correlation information is then contained in one complex correlation function, namely,

$$G(\vec{R}, \vec{R}') = \langle e^{2\pi i (s_{\vec{R}'} - s_{\vec{R}})/3} \rangle \ . \tag{2.13}$$

In a renormalization-group analysis[10] the recursion relations for decimation of all but every bth spin on a chain described by the Hamiltonian (2.2) are expressed simply as $\underline{T}' = \mathfrak{R}_b(\underline{T}) = \underline{T}^b$. This transformation may be rewritten in terms of the eigenvalues and eigenvectors of $\underline{T}$ as, simply,

$$\lambda_m' = \lambda_m^b, \ (\vec{e}^{R,m})' = \vec{e}^{R,m}, \text{ and } (\vec{e}^{L,m})' = \vec{e}^{L,m} \ . \tag{2.14}$$

III. THREE-STATE CHIRAL MODEL

The simplest model with a Hamiltonian of form (2.2) which exhibits spatially modulated correlations is a three-state model with threefold cyclic symmetry, but with a broken reflection or exchange invariance. We will call this model the *three-state chiral model.*

On a linear chain the Hamiltonian of the three-state chiral model is

$$\mathcal{H} = -\sum_i \Big[J_0 \sum_{k=0}^{2} P_i^k P_{i+1}^k + J_1 (P_i^0 P_{i+1}^1 + P_i^1 P_{i+1}^2 + P_i^2 P_{i+1}^0) + J_2 (P_i^0 P_{i+1}^2 + P_i^2 P_{i+1}^1 + P_i^1 P_{i+1}^0) \Big] . \quad (3.1)$$

The significance of each term here is best understood by examining the ground states of the system in which that particular term dominates. The term with coefficient J_0 is the usual Potts interaction; if $J_1 = J_2$ the model reduces to the usual three-state Potts model with coupling $J = J_0 - J_1$. For $J_0 > J_1$ and $J_0 > J_2$ the Potts term dominates and the ground state of the system is that of the ferromagnetic Potts model in which all spins take the same value. However, when $J_1 > J_0$ and $J_1 > J_2$ the second term in the Hamiltonian dominates and the ground state is described by

$$s_{i+n} = s_i + n \,(\mathrm{mod}\ 3) \ . \quad (3.2)$$

If the three values of s_i are thought of as three orientations of a vector in a plane normal to the chain, this ground state has a chirality that we may call *right handed.* Conversely, if $J_2 > J_1$ and $J_2 > J_0$ the ground state is similar, though of opposite, or left handed chirality.

The transfer matrix for this Hamiltonian is cyclic with first-row elements

$$T_{0m} \equiv T_m = \exp\{K_m\}, \quad m = 0, 1, 2 \ . \quad (3.3)$$

It has one real eigenvalue,

$$\lambda_0 = \sum_{m=0}^{2} T_m \ , \quad (3.4)$$

and a complex conjugate pair, namely,

$$\lambda_2^* = \lambda_1 = \sum_{m=0}^{2} T_m e^{2\pi i m/3} \ . \quad (3.5)$$

The energy zero will be chosen so that $\lambda_0 = 1$. Then the reduced Hamiltonian,

$$\bar{\mathcal{H}}(\lambda) = -\beta \mathcal{H} = \sum_i \sum_{k=0}^{2} \sum_{l=0}^{2} K_m(\lambda) P_i^k P_{i+1}^l \ , \quad (3.6)$$

where $m = l - k$ (mod 3), is fully specified by the single eigenvalue, $\lambda \equiv \lambda_1$, in terms of which the transfer matrix elements are

$$T_m(\lambda) = e^{K_m(\lambda)} = \tfrac{1}{3}(1 + e^{-2\pi i m/3}\lambda + e^{2\pi i m/3}\lambda^*) \ , \quad (3.7)$$

Due to the restriction $T_m \geq 0$, $(m = 0, 1, 2)$, all physically realizable values of λ are found to lie on or within the equilateral triangle in the complex λ plane with vertices at $e^{2\pi i m/3}$ $(m = 0, 1, 2)$ (see Fig. 1). This triangle seems to be the most natural domain in which to represent phase diagrams for the three-state chiral model. The coordinates of a point in this triangle may be expressed in two useful ways. The first is, simply, as the real and imaginary parts of the eigenvalue λ. On the other hand, if the altitude of the triangle is of unit length then the distances between a point and the three sides of the triangle are the transfer matrix elements, T_0, T_1, and T_2, corresponding to that point.

An analogy with the ANNNI model may be noticed if one rewrites the Hamiltonian (3.1) as

$$H = -J \sum_i \Big[E_0 + \sum_{k=0}^{2} P_i^k P_{i+1}^k + \kappa (P_i^0 P_{i+1}^1 + P_i^1 P_{i+1}^2 + P_i^2 P_{i+1}^0 - P_i^0 P_{i+1}^2 - P_i^2 P_{i+1}^1 - P_i^1 P_{i+1}^0) \Big] . \quad (3.8)$$

Then for $|\kappa| > 1$ the ground state has modulated order, while for $|\kappa| < 1$ it is ferromagnetic. In the ANNNI model (2.3) the ground state has modulated order for $\kappa > \frac{1}{2}$ and is ferromagnetic for $\kappa < \frac{1}{2}$.[3] The correspondence between points in the phase triangle and those in the $(k_B T/J, \kappa)$ plane is indicated in Fig. 2.

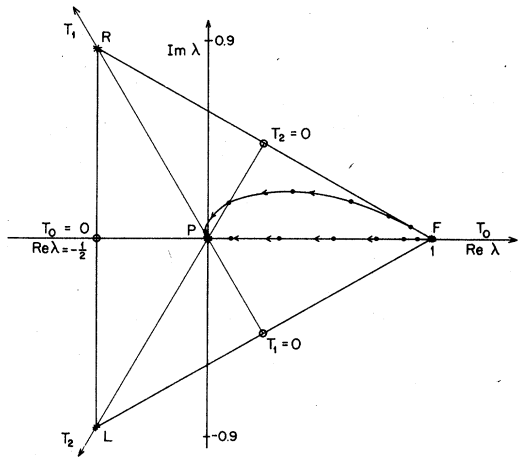

FIG. 1. The basic phase diagram of the one-dimensional three-state chiral model in the complex λ plane, where λ is the nontrivial eigenvalue of the transfer matrix. The system orders only at the points labeled F, R, and L with ferromagnetic, right-handed-chiral, and left-handed-chiral order, respectively. Under renormalization-group transformation all other points in the phase diagram are attracted to the paramagnetic fixed point, P, at which all nontrivial correlations vanish. Two flow trajectories illustrating this for a $b = 2$ renormalization group are shown.

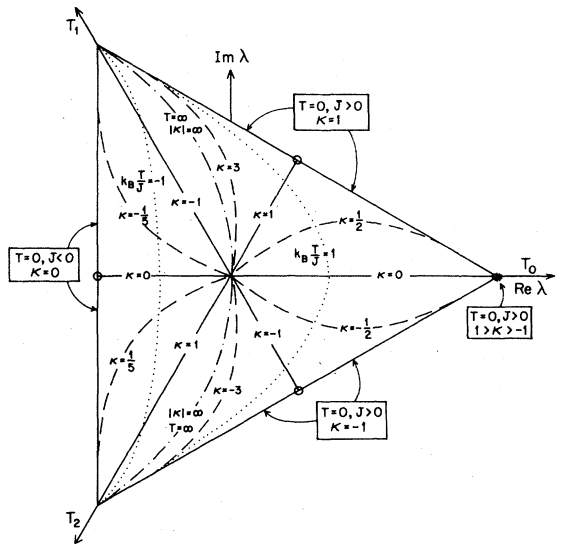

FIG. 2. The basic phase diagram in the λ plane showing the axes of the parameters T_0, T_1, and T_2 [see the relations (3.5) and (3.7)] and contours of constant k_BT/J (dotted curves) and constant κ (dashed curves) following from relations (7.1) and (7.2). Note that the mapping is singular on the edges of the triangle and on the locus $T=\infty$. Specifically, each vertex of the λ triangle maps into a line in the $T\kappa$ plane while each edge of the λ triangle maps onto a single point in the $T\kappa$ plane. Thus the multiphase behavior that is concentrated at a single *multiphase point* in the $T\kappa$ plane is spread out over an entire edge of the λ triangle (compare Figs. 8 and 10 below).

By (2.12) and (2.13) the correlation function for the one-dimensional three-state chiral model is simply

$$G(n)=\lambda^n \ . \tag{3.9}$$

Thus there is long-range order only for $|\lambda|=1$. This occurs at each of the three vertices of the phase triangle; the labels F, R, and L in Fig. 1 signify ferromagnetic, right-handed-chiral, and left-handed-chiral ordering, respectively. The remainder of the phase diagram represents a paramagnetic phase with correlation function which may be written

$$G(n)=e^{-n/\xi}e^{2\pi iqn} \ , \tag{3.10}$$

where $\xi=-1/\ln|\lambda|$ is the correlation length. Thus for λ not on the positive real axis the correlations are modulated with wave number $q=\arg(\lambda)/2\pi$ and decay exponentially, with correlation length ξ. Note that $q=1/\Lambda$ where Λ is the wavelength of the modulations in units of the lattice spacing.

The renormalization-group recursion relation (2.14) for the three-state chiral model is simply $\lambda'=\lambda^b$ or equivalently, $\xi'=\xi/b$ and $q'=bq$. The fixed points are the solutions to

$$\xi=\xi/b \text{ and } q=bq+m; \quad m=0, \pm1, \pm2, \ldots; \tag{3.11}$$

these are $\xi=0$ or ∞ and $q=m/(b-1)$. Thus the chirally ordered states marked R and L in Fig. 1, with $q=\frac{1}{3}$ and $\frac{2}{3}$, are seen as fixed points only when $b=3m+1, m=1,2, \ldots$. A similar restriction on b has been noticed for the linear chain Ising antiferromagnet.[10] On the other hand, the high-temperature disordered point and the ferromagnetically ordered state, marked P and F, respectively, in Fig. 1, appear as fixed points for any b.

IV. SYMMETRIES OF THE THREE-STATE CHIRAL MODEL

Consider a three-state model on a general d-dimensional *layered* lattice. Identify each spin by its position vector $\vec{R}_n$, where the index n indicates that the spin is in the nth layer of the lattice. The reduced Hamiltonian is

$$\bar{\mathcal{H}}(K_\perp,\lambda)=\sum_n\left[\sum_{\langle \vec{R}_n,\vec{R}'_n\rangle}K_\perp\sum_{j=0}^{2}P^j_{\vec{R}_n}P^j_{\vec{R}'_n}+\sum_{\langle R_n,R_{n+1}\rangle}\sum_{k=0}^{2}\sum_{l=0}^{2}K_m(\lambda)P^k_{\vec{R}_n}P^l_{\vec{R}_{n+1}}\right], \tag{4.1}$$

where $m=l-k$ (mod 3), and the two sums run over all nearest-neighbor pairs within the nth layer and over all nearest-neighbor pairs with one spin in the nth layer and one in the $(n+1)$st layer, respectively. The couplings $K_m(\lambda)$ are as defined in (3.7) and we assume the in-layer coupling $K_\perp$ is positive, i.e., ferromagnetic, to avoid frustration effects. The correlation function (2.13) may conveniently be written as

$$G(\vec{R}_n,\vec{R}_m;K_\perp,\lambda)=F(\vec{R}_n,\vec{R}_m;K_\perp,\lambda)e^{i\phi(\vec{R}_n,\vec{R}_m;K_\perp,\lambda)} \ , \tag{4.2}$$

where the functions F and ϕ are real.

One symmetry of this model is exhibited by relabeling all the spins so that $s_{\vec{R}}\to s'_{\vec{R}}=-s_{\vec{R}}$ (mod 3). The results of this transformation on the Hamiltonian and the correlation functions are $\lambda\to\lambda'=\lambda^*$ and $G\to G'=G^*$. Thus we conclude that

$$G(\vec{R}_n,\vec{R}_m;K_\perp,\lambda^*)=G^*(\vec{R}_n,\vec{R}_m;K_\perp,\lambda) \ . \tag{4.3}$$

Clearly, when λ is real the correlation function is always real. If λ is positive and real the system is just a three-state Potts model with ferromagnetic cou-

plings. The correlation function will then be non-negative everywhere so that $\phi = 0$. If λ is negative and real we have a Potts model with antiferromagnetic interlayer coupling. In this case we choose

$$\phi(\vec{R}_n, \vec{R}_m) = (m - n)\pi \ , \tag{4.4}$$

so that the function F remains non-negative.

The other symmetry of the model is exhibited by relabeling the spins so that $s_{\vec{R}_n} \to s'_{\vec{R}_n} = s_{\vec{R}_n} + n$ (mod 3). The results of this transformation are $\lambda \to \lambda' = \lambda \exp(2\pi i/3)$ and

$$G(\vec{R}_n, \vec{R}_m) \to G'(\vec{R}_n, \vec{R}_m) = G(\vec{R}_n, \vec{R}_m) e^{2\pi i(m-n)/3} \ , \tag{4.5}$$

from which we may conclude

$$G(\vec{R}_n, \vec{R}_m; K_\perp, \lambda e^{2\pi i/3}) = G(\vec{R}_n, \vec{R}_m; K_\perp, \lambda) e^{2\pi i(m-n)/3} \ . \tag{4.6}$$

From (4.3) and (4.6) we see that the correlation functions at the six points in the phase diagram $\lambda = |\lambda| e^{\pm i\theta}$, $\lambda = |\lambda| e^{\pm i\theta + 2\pi i/3}$, and $\lambda = |\lambda| e^{\pm i\theta - 2\pi i/3}$ are simply related. Thus the phase diagram has a sixfold symmetry and one need study only one sextant, for example just $\lambda = |\lambda| e^{i\theta}$ with $0 \leq \theta \leq \pi/3$. This sixfold symmetry is a generalization of the two-fold symmetry relating the Ising ferromagnet and antiferromagnet on a bipartite lattice in zero field. Further, we see that for $\lambda = |\lambda| e^{\pi i l/3}$ with $l = 0, \ldots, 5$, the phase of the correlation function satisfies

$$\phi(\vec{R}_n, \vec{R}_m; K_\perp, \lambda) = 2\pi(m - n) q(K_\perp, \lambda) \ , \tag{4.7}$$

with $q(K_\perp, \lambda) = l/6$ being the wave number of the modulations in the correlation function. Note that the wave *vector* of these modulations is normal to the layers, as would be expected.

In a high-temperature expansion ($|\lambda| \ll 1$) of the correlation function, we find in leading (nonvanishing) order in $|\lambda|$ the behavior

$$G(\vec{R}_n, \vec{R}_m; K_\perp, \lambda) \approx \tilde{F}(\vec{R}_n, \vec{R}_m; K_\perp, |\lambda|) \lambda^{m-n} \ , \tag{4.8}$$

where the function F is real everywhere. In the one-dimensional system, as was shown above in (3.9), we have $F = 1$, and all higher-order terms vanish. To summarize, then, we find that for all λ in the one-dimensional system, for $|\lambda| \ll 1$, and for $\lambda = |\lambda| e^{\pi i l/3}$ in any dimensionality, the relation (4.7) is valid, with $q(K_\perp, \lambda) = \arg(\lambda)/2\pi$, independent of the in-layer coupling strength $K_\perp$. This therefore indicates that (4.7) is possibly always valid for a *layered* lattice such as we are considering; in that case (4.7) serves to define the function $q(K_\perp, \lambda)$ unambiguously. However, we must be cautious on this point because of the counterexample provided by the "mock ANNNI models"[19] where the correlation function has competing periodicities and q can only be defined uniquely by specifying that it refers to the *primary,* or strongest component in the spatial modulations of the correlation function, a somewhat less practical definition to use. If, as we suspect, (4.7) is not always valid in the present model, the wave number $q(K_\perp, \lambda)$ may likewise be defined as that of the maximum or the strongest Bragg peak in the structure factor:

$$S(q; K_\perp, \lambda) = N^{-1} \sum_n \sum_{\vec{R}_n} \sum_m \sum_{\vec{R}_m} e^{2\pi i q(n-m)} G(\vec{R}_n, \vec{R}_m; K_\perp, \lambda) \ , \tag{4.9}$$

where N is the number of sites in the lattice. In any case we expect that $q(K_\perp, \lambda)$ at least roughly corresponds to the modulations in the correlation function, i.e., that

$$G(\vec{R}_n, \vec{R}_m; K_\perp, \lambda) \simeq F(\vec{R}_n, \vec{R}_m; K_\perp, \lambda) e^{2\pi i(m-n) q(K_\perp, \lambda)} \tag{4.10}$$

represents, physically, a good description.

If, considered by itself, each layer of sites and in-layer bonds is a well-connected lattice of dimensionality $d > 1$, it appears that a systematic low-temperature series expansion might be generated for the model in a manner following Fisher and Selke's treatment of the ANNNI model for $d > 2$.[5] One would expect, as with the ANNNI model, that the system would always order at sufficiently low temperatures. However, to avoid explicit spatial anisotropy in the Hamiltonian, which complicates a renormalization-group treatment, we turn now to the three-state chiral model on a hypercubic lattice in a special case where there are *no* in-layer couplings ($K_\perp \equiv 0$); this is a system whose low-temperature behavior is rather less obvious but which, as we will indicate, will still exhibit phases with well-defined layered ordering.

V. MIDGAL-KADANOFF RENORMALIZATION GROUP

In this section we specify the recursion relations that will be studied for a special three-state chiral model on a d-dimensional hypercubic lattice and point out that they are an *exact* dedecoration renormalization group[10] for the same model on a certain class of "fractals" or hierarchical pseudolattices.[13–16]

To specify the model on a hypercubic lattice let the basic lattice vectors be $\vec{a}_i (i = 1, \ldots, d)$. To achieve the maximum simplicity all bonds in the lattice will

be assigned the same coupling strength, the model thus being spatially isotropic, in a definite sense. However, the interactions themselves are not reflection symmetric, so we may define layers in the system; these will be taken as the lattice planes normal to the principal diagonal vector

$$\vec{n} = \sum_{i=1}^{d} \vec{a}_i \ . \tag{5.1}$$

Each nearest-neighbor pair in the lattice thus consists of spins in two adjacent layers. The reduced Hamiltonian to be considered is expressed simply by

$$\overline{\mathcal{H}} = \sum_{\vec{R}} \sum_{i=1}^{d} \sum_{k=0}^{2} \sum_{l=0}^{2} K_{l-k\,(\mathrm{mod}\,3)} P^{k}_{\vec{R}} P^{l}_{\vec{R}+\vec{a}_i} \tag{5.2}$$

in which no direct in-layer interactions appear.

A simple approximate renormalization group may be generated easily for this Hamiltonian by using the bond-moving procedure of Kadanoff.[11,12] The resulting recursion relations for a lattice rescaling factor, b, are

$$T'_m = A \left(\sum_{k=0}^{2} T_k T_{m-k\,(\mathrm{mod}\,3)} \right)^{b^{d-1}} , \quad m = 0, 1, 2 \ , \tag{5.3}$$

where $T_m = \exp K_m$ and $A = A(T_0, T_1, T_2)$ is chosen to preserve the normalization condition

$$\sum_{m=0}^{2} T'_m = 1 \ . \tag{5.4}$$

These recursion relations map the unit λ triangle into itself. However, this map is not properly invertible, the inverse being either nonexistent or multivalued in most regions of the triangle. This noninvertibility of the renormalization-group recursion relations is an essential feature leading to the novel phase diagrams reported below.

The Migdal-Kadanoff recursion relations are, of course, approximate as applied to the hypercubic lattice Hamiltonian (5.2). However, it has been noted[13,14] that when b and b^{d-1} are both integral there is an alternative, although rather unphysical lattice structure for which these renormalization-group recursion relations are exact. This pseudolattice or fractal[15,16] lattice is generated from a simple graph of two sites connected by a bond through an infinite number of repeated applications of the following two steps: (i) Replace every bond in the lattice with b^{d-1} parallel bonds; and (ii) decorate every bond in the new lattice with $(b-1)$ new sites. A section of this lattice for the case $b = d = 2$ is shown in Fig. 3. The majority of the sites have coordination number $z = 2$, but there are sites in the lattice with coordination number $z_k = 2^k$ where k becomes arbitrarily large. Thus the lattice is not fully homogeneous or translationally invariant; nevertheless it is important in understanding the behavior of the recursion relations (5.3) to note

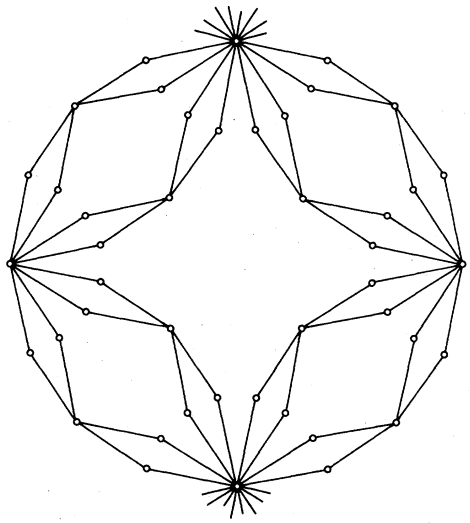

FIG. 3. A section of the hierarchical or fractal lattice for which the Migdal-Kadanoff renormalization group is exact. The case $b = d = 2$ is illustrated.

that the lattice displays effective periodicities of a hierarchical nature. The set of sites with $z \geq 2b^{n(d-1)}$, for n integral, constitute a superlattice that consists of every b^nth "layer" of the original lattice. For every integer n, therefore, there is an effective periodicity in the lattice of b^n lattice bonds. It can be seen that the sites of very high coordination number play an important role in keeping the modulated order always locked commensurately to the lattice structure. In the hypercubic lattice there are, of course, no sites of anomalously high coordination number so truly incommensurate phases are more likely to occur. However they cannot be found by using the simple recursion relations (5.3).

Since the recursion relations (5.3) are exact for a certain layered lattice structure they must respect the full symmetries of the model as discussed above, and embodied in (4.3) and (4.6). Let the recursion relations be written as

$$\lambda' = \mathfrak{R}_{b,d}(\lambda) \ , \tag{5.5}$$

where λ is defined by (3.5), as before. The symmetry (4.3) is respected in that

$$\mathfrak{R}(\lambda^*) = [\mathfrak{R}(\lambda)]^* \ , \tag{5.6}$$

from which it follows that if λ_0 is a fixed point then λ_0^* is also a fixed point. The symmetry (4.6) is also respected because

$$\mathfrak{R}_{b,d}(\lambda e^{2\pi i/3}) = e^{2\pi i b/3} \mathfrak{R}_{b,d}(\lambda) \ . \tag{5.7}$$

Thus, in the case $b = 2$, if λ_0 is a fixed point then $\lambda_0 e^{\pm 2\pi i/3}$ are not individual fixed points, but together

make up a *fixed cycle* of period two iterations. We will in fact find fixed cycles of all periods in this model.

This renormalization group may be linearized about a fixed point λ_c in the standard way.[10,20] The resulting linear operator has just two eigenvalues, Λ_0 and Λ_1. From (5.6) we find that the eigenvalues of the renormalization group linearized about the fixed point λ_c^* are Λ_0^* and Λ_1^*. But since the Λ_i are roots of a real quadratic equation, either both are real, in which case $\Lambda_i = \Lambda_i^*$, or else one has $\Lambda_0 = \Lambda_1^*$. In either case the eigenvalues at the fixed points λ_c and λ_c^* are identical. Similar reasoning, using Eq. (5.7), shows that the eigenvalues of the renormalization group with $b=2$ at either of the two fixed cycles of period two, $\lambda_c e^{\pm i2\pi/3}$ or $\lambda_c^* e^{\pm i2\pi/3}$, are also the same as those at λ_c. These four fixed cycles, two of period two and two of period one, thus have the same eigenvalues and occur at points in the phase diagram that are equivalent under the symmetries (4.3) and (4.6). They constitute what we will call a *class of fixed cycles,* i.e., a set of fixed cycles which are equivalent under either (5.6) or (5.7) and which thus have the same eigenvalues. Note that all such classes of fixed cycles will contain at least one "vertex," or point in the cycle, in each sextant of the λ phase diagram. Thus, again, one need examine only a single sextant of the phase diagram: what is found there will simply be repeated in the other five sextants.

Because the recursion relations (5.3) operate in a two-dimensional parameter space, (the complex λ plane) the renormalization group linearized about a fixed cycle has only two eigenvalues. Thus there are three main types of stability possible for a given fixed cycle. It is an *attractor* if both eigenvalues are less than unity, it is *critical* if one eigenvalue is less than unity and the other is greater than unity, and it is *multicritical* if both eigenvalues exceed unity.

We turn now to the construction and analysis of the phase diagrams following from the recursion relations (5.3).

VI. FIXED POINTS AND PHASE DIAGRAMS

The renormalization-group recursion relations (5.3) have been studied numerically and analytically for $b=2$ and for various values of the dimensionality parameter d: the results are reported in this and the following section.

As seen in the one-dimensional case ($d=1$), there are always two trivial fixed points, namely $\lambda=0$ and $\lambda=1$. The former, P, is an attractor for all d: the set of all points in the phase diagram that are attracted to it under repeated iteration of the recursion relations represents the disordered, or paramagnetic phase. The fixed point, F, at $\lambda=1$ (or $T_0=1$, $T_1=T_2=0$) is an attractor for $d>1$ and represents the fully ordered ferromagnetic state. This fixed point is located in one corner of the triangular phase diagram (see Fig. 1). The other two corners, representing the states with maximal or saturated chiral order, make up a fixed cycle of period two under the $b=2$ recursion relations which is also an attractor for $d>1$. These two classes of attractors, the disordered point $\lambda=0$ which is in a class by itself and the ordered fixed cycles $\lambda=1$ and $\lambda=e^{\pm 2\pi i/3}$, are the only attractors present in the model: both have eigenvalues $\Lambda_0=\Lambda_1=0$ for $d>1$.

Let us now restrict attention to $d>1$; there is then a region of the phase diagram containing the attractor $\lambda=1$ which represents an ordered phase with nonmodulated or simple ferromagnetic order. This follows because all points in this phase approach, under the discrete action of the recursion relations, the fixed point $\lambda=1$ on a quasismooth trajectory lying totally within the phase (see, e.g., solid points 3, 4, 5 . . . in Fig. 4). On the boundary of this phase there are three fixed points which are labeled C_0, C^+, and C^- in Fig. 5, where the phase diagram, constructed numerically, is exhibited for $d=2$. The

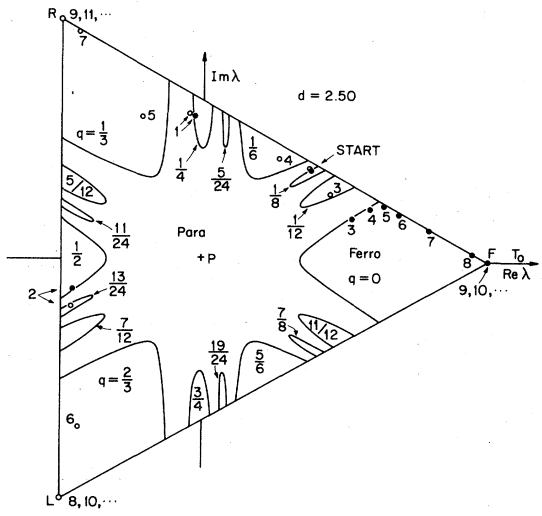

FIG. 4. Phase diagram for $d=2.50$ showing the major classes of ordered phases (see also Fig. 8 below) and illustrating some (discrete) trajectories under the $b=2$ renormalization group. The label "START" marks the initial points, one with $q_0=\frac{1}{8}$, the other with $q_0=\frac{13}{96}$. Successively renormalized states are labeled 1, 2, ... To identify the initial phases first follow the trajectory of the open circles backwards: point 5 has $q_5=\frac{1}{3}$ and so point 4 has $q_4=\frac{1}{6}$ and point 3 has $q_3=\frac{1}{12}$. Point 2 could have $q_2=\frac{1}{24}$ or $\frac{13}{24}$ but in view of its location the latter is clearly correct. Continuing two steps further gives $q_0=\frac{13}{96}$. All points within the $q=\frac{1}{8}$ phase map, after three steps, into the $q=0$ phase in a fashion similar to the sequence of solid circles illustrated.

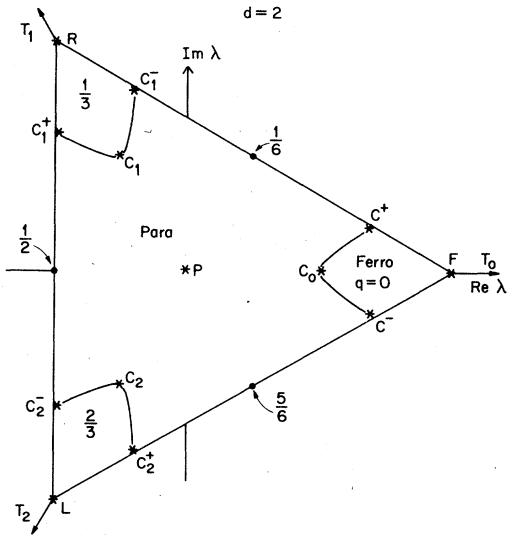

FIG. 5. Phase diagram of the three-state chiral model on the $b=2$, $d=2$ lattice illustrated in Fig. 3. There are six distinct ordered phases. Note that the critical fixed points C_i^+ and $C_i^-(i=0,1,2)$ lie just *inside* the triangle.

fixed point C_0 is on the real (or $T_1=T_2$) axis and represents the critical point of the standard three-state Potts model. In the context of the present system this is a multicritical fixed point. All other points on the boundary of this ferromagnetically ordered phase are attracted to either C^+ or C^-, those in the lower half plane to C^- and those in the upper half plane to C^+. These two critical fixed points belong to the same class; if C^+ is located at λ_c then C^- is at λ_c^*. The five fixed points P, F, C_0, and $C^\pm$ are the only fixed *points* found in this model. Their eigenvalues are reported in Table I.

By the symmetry (4.6) we know that there must be chirally ordered phases similar to the ferromagnetic phase but located in the other corners of the λ triangle (see Figs. 4 and 5). In anticipation of a proliferation of different chirally ordered phases we introduce here a systematic method for characterizing the nature of the order in these phases.

The identification of the different ordered phases is based upon the hypothesis, embodied in Eq. (4.10), that for every point in the phase diagram there is a wave number $q(\lambda)$ that characterizes the spatial modulations in the two site correlation function (2.13). In the following we explicitly construct the function $q(\lambda)$. Because of the discrete nature of the lattice the wave number $q(\lambda)$ may always be chosen to be within the "first Brillouin zone," which will be taken as $0 \leq q < 1$. Under application of the $b=2$ renormalization group the lattice is rescaled by a factor of 2 so we have

$$q(\lambda) \rightarrow q(\lambda') = 2q(\lambda) - [2q(\lambda)] \ , \tag{6.1}$$

where $[x]$ denotes the integral part of x. The inverse of this transformation is evidently double valued; one has *either*

$$q(\lambda) = q(\lambda')/2 \ , \tag{6.2a}$$

or

$$q(\lambda) = [q(\lambda') + 1]/2 \ . \tag{6.2b}$$

Assuming $q(\lambda')$ is known, this ambiguity in $q(\lambda)$ will be removed by asserting a weak "monotonicity" in $q(\lambda)$. It was proven above that on the line $\lambda = |\lambda|$ one has $q(\lambda)=0$, while on the line $\lambda = |\lambda| e^{\pi i/3}$, one has $q(\lambda) = \frac{1}{6}$. These two lines enclose the first sextant of the phase diagram, within which we assume $0 \leq q(\lambda) \leq \frac{1}{6}$. In light of the relations (4.3) and (4.6) this is equivalent to the more general assertion

TABLE I. The eigenvalues of the linearized renormalization group at the fixed points.

Fixed point	d	$\Lambda_i = 2^{y_i}$ y_0	y_1
P	Arbitrary	$-\infty$	$-\infty$
F	$d>1$	$-\infty$	$-\infty$
C_0	$1+\epsilon$	ϵ	ϵ
	2	0.83	0.42
	2.5	0.97	0.52
	3	1.03	0.62
	$d \rightarrow \infty$	1	1
$C^\pm$	$1+\epsilon$	ϵ	-1
	2	0.99	-1.7
	2.5	1.50	-3.0
	3	2.00	-4.9
	$d \rightarrow \infty$	$d-1$	$-\infty$

that if $\lambda = |\lambda| e^{i\phi}$, where

$$m/6 < \phi/2\pi < (m+1)/6 \ , \tag{6.3}$$

in which m is an integer, then one has

$$m/6 \leq q(\lambda) \leq (m+1)/6 \ . \tag{6.4}$$

This conclusion is certainly valid in a mean-field-theory treatment of the system, as well as in the high-temperature expansion discussed above: see (4.8). As will be shown, the relations (6.1) to (6.4) together with the recursion relation (5.5) serve to determine the wave number $q(\lambda)$, in principle, to arbitrary accuracy for all $\lambda(\neq 0)$, within the phase diagram. Thus we construct a well-defined function $q(\lambda)$ that, for $d=1$ as well as for arbitrary d provided $\lambda = |\lambda| e^{im\pi/3} (m = 0, 1, \ldots, 5)$, is *precisely* the wave number of the modulations in the correlation function as defined by Eq. (4.7). Otherwise the correspondence is not quite so precise, but there is every indication that $q(\lambda)$ does effectively characterize the modulations in the correlation function at large distances in the sense of Eq. (4.10).

There are two steps in the procedure for determining the wave vector $q(\lambda)$: first, the recursion relations are iterated until a point $\lambda_n = \mathcal{R}^n(\lambda)$ is reached at which either $q(\lambda_n)$ is already known or n is sufficiently large. Then, using relation (6.2), $q(\lambda_{n-1})$ is determined from $q(\lambda_n)$, $q(\lambda_{n-2})$ from $q(\lambda_{n-1})$, . . . , and finally $q(\lambda)$ is determined from $q(\lambda_1)$. Note that if $q(\lambda_{l+1})$ is known to be in an interval of width ϵ_{l+1}, i.e., $q_{l+1} \leq q(\lambda_{l+1}) \leq q_{l+1} + \epsilon_{l+1}$, then, from (6.2), $q(\lambda_l)$ is known to lie in an interval of width $\epsilon_l = \frac{1}{2}\epsilon_{l+1}$. Thus, if $q(\lambda_n)$ is not known, we have $\epsilon_n = \frac{1}{6}$ from (6.4) and by the above procedure $q(\lambda)$ is determined to lie in an interval of width $\epsilon_0 = 2^{-n}/6$ which may be made arbitrarily small by choosing n sufficiently large.

The points in the phase diagram that represent ordered phases with modulations commensurate with the lattice are all attracted to a fixed cycle under repeated iteration of the recursion relations. For these points $q(\lambda)$ is certainly known exactly, because the wave number $q(\lambda_v)$ at a vertex, v, of a fixed cycle is uniquely determined by the above procedure. If the fixed cycle closes after n steps we have $q(\lambda_v) = 2^n q(\lambda_v) - m$ (m integral) so that $q = m/(2^n - 1)$. By noting in which sextant of the phase diagram each vertex of the fixed cycle is located one can determine each $q(\lambda_v)$ explicitly.

For low enough dimensionality ($d \lesssim 2.12$) one finds numerically that the only classes of fixed cycles present are the four previously mentioned, represented in the first sextant by P, F, C_0, and C^+ (see Fig. 5). By the above reasoning the fixed *points* representing ordered states (F, C_0, and $C^{\pm}$) have wave number $q=0$. They are all located either within or on the phase boundary of the ferromagnetically ordered phase, which must therefore be identified as the $q=0$ phase. For each of these fixed points, located at, say, λ_c, there is a fixed cycle of period two in the same class with vertices at $\lambda_c e^{\pm 2\pi i/3}$. Each such vertex is located within or on the boundary of one of the two chirally ordered phases (with $q = \frac{1}{3}$ and $\frac{2}{3}$) which, by the symmetry (4.6), are similar to the $q=0$ phase. In Fig. 5 the Potts-like fixed cycle of period two, which is in the same class as the Potts multicritical point C_0, is labeled by C_1 and C_2. Similarly, there are two other fixed cycles, $C_1^{\pm}$ and $C_2^{\pm}$, that attract all other points on the $q = \frac{1}{3}$ and $q = \frac{2}{3}$ phase boundaries and are in the same class as C^+ and C^-. Under a single iteration of the recursion relations the $q = \frac{1}{3}$ phase maps into the $q = \frac{2}{3}$ phase and vice versa. The three ordered phases with $q = 0$, $\frac{1}{3}$, and $\frac{2}{3}$ are in the same class, in that they occupy equivalent regions of the phase diagram. In general, if there is an ordered phase with modulations of wave number $q = q_0$, the symmetries (4.3) and (4.6) dictate that there will also be phases of the same class with wave numbers $q = (\frac{1}{3} \pm q_0)$, $(\frac{2}{3} \pm q_0)$, and $(1 - q_0)$. We will identify each such class of phases by the wave number of its representative in the first sextant of the phase diagram.

For dimensionality $d < 2$ one finds only this single class of ordered phases. The remainder of the phase diagram represents the disordered or paramagnetic phase. However, one can show analytically that at $d=2$ a class of three new phases appears, with $q = \frac{1}{6}$, $\frac{1}{2}$, and $\frac{5}{6}$. For $d=2$ these phases exist only at single critical points on the edge of the phase diagram, namely, $\lambda = \frac{1}{2} e^{2\pi i q}$ (see Fig. 5). As is readily checked analytically, under one iteration of the recursion relations the $q = \frac{1}{2}$ critical point, for example, is mapped to C_0, the Potts multicritical point. Similarly, the other new critical points, with $q = \frac{1}{6}$ and $\frac{5}{6}$, are mapped onto the Potts-like fixed cycle of period two, C_1, C_2. For $d > 2$ these new phases expand to occupy finite areas in the phase diagram. Thus $d = d^*(\frac{1}{6}) = 2$ is the borderline dimension for this new class of phases, at which they first appear, occupying only a single critical point on the edge of the phase diagram. By the same token, the borderline dimension for the original class of ordered phases is $d^*(0) = 1$.

As d increases further one discovers numerically that new classes of phases keep appearing. The third class of ordered phases, with $q = \frac{1}{12}$, $\frac{1}{4}$, $\frac{5}{12}$, $\frac{7}{12}$, $\frac{3}{4}$, and $\frac{11}{12}$, has a critical dimension estimated numerically as just under $d = 2.10$. The first sextant of the phase diagram for $d = 2.10$ is shown in Fig. 6. Under iteration of the recursion relations the $q = \frac{1}{12}$ phase maps into the $q = \frac{1}{6}$ phase, which in turn maps into the $q = \frac{1}{3}$ phase. Similarly, the phase boundary of

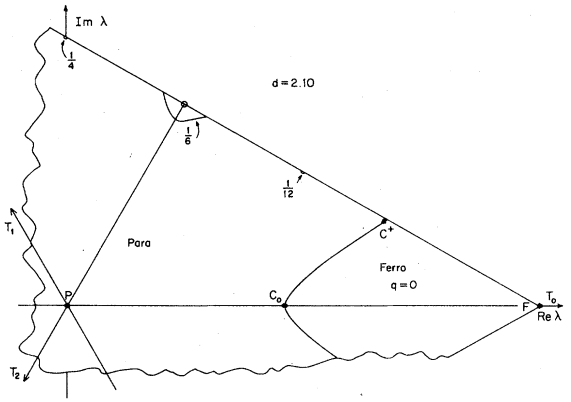

FIG. 6. A portion of the phase diagram for $d=2.10$. The $q=\frac{1}{12}$ and $\frac{1}{4}$ phases have now appeared, as have the $q=\frac{5}{12}$, $\frac{7}{12}$, $\frac{3}{4}$, and $\frac{11}{12}$ phases (although these are not shown).

the $q=\frac{1}{12}$ phase maps after two iterations into the phase boundary of the $q=\frac{1}{3}$ phase.

All points in phases with true long-range order must be attracted to a zero temperature attractor [F or (R,L)] upon sufficient iteration of the renormalization group. Each such point, λ, must therefore satisfy $\mathcal{R}^n(\lambda)=\lambda_n$, for some n, where λ_n is a point within a member of the original class of ordered phases, i.e., $q(\lambda_n)=\frac{1}{3}m$ (m integral). Thus we find that the wave number identifying a phase with true long-range order must satisfy $q=m2^{-n}/3$, where m and n are integers, with m odd. The $q=m2^{-n}/3$ phase maps, under $\mathcal{R}^n$, into the $q=m(\mathrm{mod}3)/3$ phase.

The general character of the "trajectories" under the recursion relations is illustrated in Fig. 4, which shows two examples for $d=2.50$. Four different classes of ordered phases are also shown in this figure. The solid point marked "START" is in the $q=\frac{1}{8}$ phase and, after three iterations, is mapped into the $q=0$ phase, passing through the $q=\frac{1}{4}$ and $\frac{1}{2}$ phases on the way. In no sense can a smooth "flow" be drawn through the first four points on this trajectory; however after arriving in the $q=0$ phase the trajectory does become quite smooth. The open point marked "START" just outside the $q=\frac{1}{8}$ phase, is actually in the very slender $q=\frac{13}{96}=13(2^{-5})/3$ phase, whose boundary is not drawn in Fig. 6. After five iterations of the recursion relations this point is mapped into the $q=\frac{1}{3}$ phase, passing through the $q=\frac{13}{48}$, $\frac{13}{24}$, $\frac{1}{12}$, and $\frac{1}{6}$ phases on the way. It is subsequently attracted to the zero temperature fixed cycle of period two (R,L), all the while jumping back and forth between the $q=\frac{1}{3}$ and $\frac{2}{3}$ phases.

Since the mapping $\mathcal{R}^n$ is continuous the boundary of the $q=m2^{-n}/3$ phase maps under $\mathcal{R}^n$ into the phase boundary of a member of the original class of ordered phases. Thus all $q=m2^{-n}/3$ phase boundaries are governed by just two classes of fixed cycles. There is at most one multicritical point on the boundary of each ordered phase that is attracted to a Potts-like fixed cycle. The critical behavior at each such Potts-like multicritical point is the same as that at the fixed point C_0, the critical point of the Potts model. The remainder of each phase boundary is governed by the class of fixed cycles represented in the first sextant by C^+. The one relevant eigenvalue at these fixed cycles is numerically well approximated by $\Lambda_0\simeq 2^{d-1}$ for all $d>1$. Therefore, everywhere on each phase boundary except at the Potts-like multicritical point the specific heat (or other appropriate susceptibility) is singular with the critical exponent satisfying

$$\alpha\simeq-\frac{d-2}{d-1}\ . \tag{6.5}$$

In the vicinity of each Potts-like multicritical point there is a crossover between the two types of critical behavior. The crossover exponent satisfies

$$\phi_P=\frac{\ln\Lambda_1}{\ln\Lambda_0}<1 \tag{6.6}$$

(see Table I) so that all phase boundaries remain smooth with a continuous tangent at the Potts-like multicritical points.

One finds numerically that as d is increased beyond $d=2.10$ new phases appear in large numbers. In fact, as we will demonstrate, the number of distinct ordered phases diverges at a critical dimension, d_1, estimated numerically as $d_1\simeq 2.125$. The qualitative mechanism for this is illustrated in Fig. 7, where a small portion of the phase diagram containing the fixed point C^+ is shown for dimensionalities just below and just above d_1. The renormalization group may be linearized about the fixed point C^+ simply as

$$(x,y)\rightarrow(x',y')=(\Lambda_1 x,\Lambda_0 y)\ , \tag{6.7}$$

where the x and y axes represent the scaling axes and $\Lambda_0>1>\Lambda_1$. The x axis is simply the boundary of the $q=0$ phase, while the y axis is *roughly* parallel to the edge of the phase diagram, which represents zero temperature (recall Fig. 2). For $d<d_1$ the y axis does not intersect any ordered phases. The point in the $q=2^{-n}/3$ phase that is closest to the y axis is (x_n,y_n). From the linearized recursion relations we see that the point in the $q=2^{-m}/3$ phase that is closest to the y axis is

$$(x_m,y_m^i)=(x_n/\Lambda_1^{m-n},\ y_n/\Lambda_0^{m-n})\ . \tag{6.8}$$

But the edge of the phase diagram is roughly at

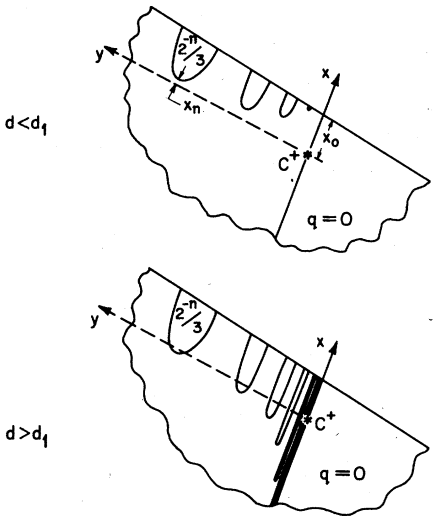

FIG. 7. A qualitative illustration of the divergence of the number of ordered phases which occurs when d passes through d_1.

$x = x_0$. Thus for $x_m > x_0$ the $q = 2^{-m}/3$ phase is absent, being outside the phase diagram in the nonphysical region. As d increases the ordered phases grow. Let d_1 be the dimensionality at which the $q = 2^{-n}/3$ phase first intersects the y axis; for d sufficiently close to d_1 we may approximate x_n to linear order in d as

$$x_n(d) \approx X(d_1 - d) \ , \tag{6.9}$$

with $X > 0$. The borderline dimension $d^*(2^{-m}/3)$ is the dimension at which the $q = 2^{-m}/3$ phase first appears as a single point on the edge of the phase diagram and above which the $q = 2^{-m}/3$ phase is always present. For small y the edge of the phase diagram is at $x \simeq x_0$; thus for $d = d^*(2^{-m}/3)$ we have

$$x_0 \simeq x_m(d) = \Lambda_1^{n-m} x_n(d) \approx \Lambda_1^{n-m} X(d_1 - d) \tag{6.10}$$

from which we see that

$$d^*(2^{-m}/3) \approx d_1 - x_0 \Lambda_1^{n-m}/X \ . \tag{6.11}$$

Clearly, as d approaches d_1 from below the number of distinct ordered phases diverges, with all $q = 2^{-m}/3$ phases, $m = 1, 2, 3 \ldots$, appearing.

The situation for $d > d_1$ is also illustrated in Fig. 7; in the limit $m \to \infty$ the $q = 2^{-m}/3$ phase is infinitely slender and parallel to the $q = 0$ phase boundary, extending from the edge of the phase diagram all the way to the Potts fixed point, C_0.

The critical dimension d_1 is just the first of an infinite number of such critical dimensionalities. For example, there is a very similar critical dimension, d_l, for each odd integer l at which all the $q = l2^{-m}/3$ phases, $m = 1, 2, 3, \ldots$, first appear. As will be indicated in the next section, the evolution of the phase diagram as d increases is very rich in detail.

VII. EVOLUTION OF THE COMPLETE PHASE DIAGRAM

As the dimensionality is increased beyond d_1 new phases continue to appear. This continues until a final critical dimension, $d_f \simeq 2.625$, is reached, at which point the phase diagram appears to be complete, with an ordered phase for every rational fraction q satisfying $0 \leq q < 1$. Some features of the evolution of the phase diagram as d is increased to this final critical dimension and the resulting "complete" phase diagram are described briefly below.

One important feature is the appearance of new fixed cycles with periods of three or more iterations. To understand the origin and nature of these new fixed cycles it is helpful to consider the "q_0 *manifolds*," each of which consists of all points, λ, in the phase diagram where the wave number $q(\lambda)$, is equal to a given q_0. Under the operation of the recursion relations the q_0 manifold clearly maps into the $2q_0$ manifold. For $d = 1$ the q_0 manifold is simply the line segment $\lambda = re^{2\pi i q_0}$ $(0 < r \leq r_{\max})$, which extends from $\lambda = 0$ to the edge of the phase diagram at $\lambda = r_{\max} e^{2\pi i q_0}$. As d is increased above unity each q_0 manifold deviates from its original straight line form, though remaining in approximately the same location. For $q_0 = m2^{-n}/3$ the manifold expands, as d exceeds the borderline dimension of the $q = m2^{-n}/3$ phase, to encompass that phase and its boundary. If q_0 is irrational it appears from the numerical studies that for $d \geq d_f$ the q_0 manifold terminates at a point well short of the edge of the phase diagram. The function $q(\lambda)$ is found to be monotonic in the following sense: if q_1 and δq are rational with $0 < \delta q \ll 1$ then the q_1 manifold and the $(q_1 + \delta q)$ manifold enclose a narrow, roughly wedge-shaped region of the phase diagram that contains the q_0 manifold if and only if $q_1 < q_0 < q_1 + \delta q$.

If q_0 is a rational fraction it can be written in the form $l2^{-m}/(2^n - 1)$, with l, m, and n integers. (The proof of this is left to the reader.) The $l2^{-m}/(2^n - 1)$ manifold maps, under $\mathfrak{R}^m$, into the $k/(2^n - 1)$ manifold, where $k = l[\mathrm{mod}(2^n - 1)]$. The ordered phases described in the previous section correspond to the case $n = 2$. For $n > 2$ we find that the $k/(2^n - 1)$ manifold is a simple curve extending from $\lambda = 0$ to the edge of the phase diagram. Under $\mathfrak{R}^n$ this line maps into itself. There is a borderline dimension $d^*[k/(2^n - 1)]$ below which all points on this manifold are attracted to the paramagnetic fixed point $\lambda = 0$ upon repeated application of $\mathfrak{R}^n$. It is easily

shown that for $d < d^*[k/(2^n-1)]$ the $k/(2^n-1)$ manifold is actually contained within a (possibly extremely thin) region of the paramagnetic phase that extends out to the edge of the phase diagram. Furthermore, the $q=[k/(2^n-1)+l]/2^m$ manifold, and a region of paramagnetic phase containing it, map under $\mathfrak{R}^m$ into this region of paramagnetic phase containing the $k/(2^n-1)$ manifold. Thus as long as $d < d^*[k/(2^n-1)]$, for any k or n, there are regions of paramagnetic phase extending to the edge of the phase diagram which are dense in q space. Between any two ordered phases therefore there must be regions of paramagnetic phase.

Numerical study reveals that what happens at $d=d^*[k/(2^n-1)]$ can be described as a simple bifurcation. A new fixed point of $\mathfrak{R}^n$ appears on the $k/(2^n-1)$ manifold which has eigenvalues $\Lambda_0 > 1 = \Lambda_1$. Note that a fixed *point* of $\mathfrak{R}^n$ is a fixed *cycle* of period n under the action of $\mathfrak{R}$. For $d > d^*[k/(2^n-1)]$ this marginal fixed point of $\mathfrak{R}^n$ bifurcates into a multicritical point and a critical point. The $k/(2^n-1)$ manifold is then separated into two parts by the multicritical point. The part nearest the $\lambda=0$ fixed point is still attracted to it and remains in the paramagnetic phase. The rest of the line, however, is attracted to the new critical point and thus represents a new phase with modulated order of wave number $q=k/(2^n-1)$. This phase is confined to the one-dimensional manifold of points attracted to the new critical point so, in contrast to the $q=m2^{-n}/3$ phases, occupies a region of measure zero in the phase diagram. Apparently, all the bifurcations occur in the dimensionality range $d_1 < d \leq d_f$, the final bifurcation occurring at d_f being that associated with the fixed cycle of period six governing the $q=\frac{1}{9}, \frac{2}{9}, \frac{4}{9}, \frac{8}{9}, \frac{7}{9}$, and $\frac{5}{9}$ phases.

To summarize, for $d \geq d_f$ the renormalization-group recursion relations (5.3) appear to yield an ordered phase with modulations in the local order characterized by a wave number q for every rational fraction q. There are two distinct types of ordered phases. Those with $q=m2^{-n}/3$, where m and n are integers, occupy a finite area in the phase diagram and the points within these phases are attracted to zero-temperature fixed cycles under sufficient iteration of the renormalization group. The remainder of the ordered phases occur only on single lines in the phase diagram and the points in these phases are attracted to finite-temperature critical fixed cycles of period three or more. One would expect that the correlation function at a finite-temperature critical point might exhibit power-law decay at long distances. Thus the latter ordered phases appear to have algebraic order, in contrast to the former, which have truly long-range order.

It appears that for $d \geq d_f$ the paramagnetic phase no longer extends to the edge of the phase diagram. The phase diagram is thus divided into two regions: the paramagnetic phase in the center and a region of ordered phases around the outside. The boundary between these two regions is not a simple smooth curve since it contains a multicritical point where it intersects the q manifold for every rational fraction q. At the Potts-like multicritical points, for $q=m2^{-n}/3$, the curve is smooth, but at all the remaining multicritical points the crossover exponent appears to be greater than unity so that cusplike singularities are to be expected. Thus the boundary between ordered and disordered phases appears to be singular everywhere, because the rational numbers are everywhere dense on it.

The first sextant of the phase diagram as constructed numerically for $d=2.50$ is shown in Fig. 8. This is not really the "complete" phase diagram, but to detect the absence of certain phases requires looking at minute numerical details. For example, near the edge of the phase diagram the sliver of paramagnetic phase containing the $\frac{1}{7}$ manifold is approximately of width 10^{-9}, being hemmed in by the $q=(\frac{1}{7}+2^{-19}/21)$ and $q=(\frac{1}{7}-2^{-21}/7)$ phases on either side. In Fig. 8 the $q=m2^{-n}/3$ phases are displayed for $n \leq 4$. Note that for $n > 2$ a $q=m2^{-n}/3$ phase occupies a narrow strip of the phase diagram. For $d \gtrsim 2.5$ we find that the width of the strip is approximately proportional to $2^{-(d-1)n}$. The shaded regions in Fig. 8 are thus occupied by ordered phases too slender to resolve, as well as by others that live only on single lines. Because $d=2.50 < d_f$ there are also slender strips of paramagnetic phase between adjacent ordered phases.

The wave number $q(\lambda)$ has been calculated at intervals of 10^{-3} in $\mathrm{Im}\lambda$ along the line segment marked AB in Fig. 8, namely $\mathrm{Im}\lambda+\mathrm{Re}\lambda=0.7$. The data are exhibited in the lower trace of Fig. 9. The wave number $q(\lambda)$ has also been obtained on AB in the vicinity of the $q=0$ phase boundary at intervals of 10^{-6} in $\mathrm{Im}\lambda$. These data are exhibited in the upper

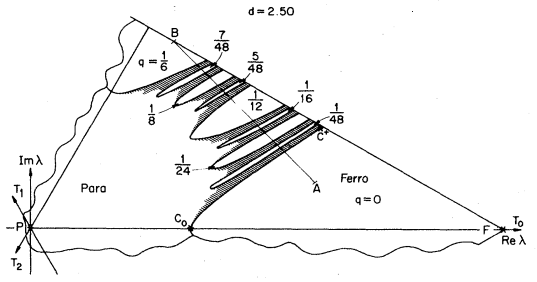

FIG. 8. Section of the phase diagram for $d=2.50$. The principle ordered phases are shown explicitly and labeled by their wave numbers. The shaded regions contain many slender ordered-phase regions and slivers of paramagnetic phase (see also Fig. 4, above.)

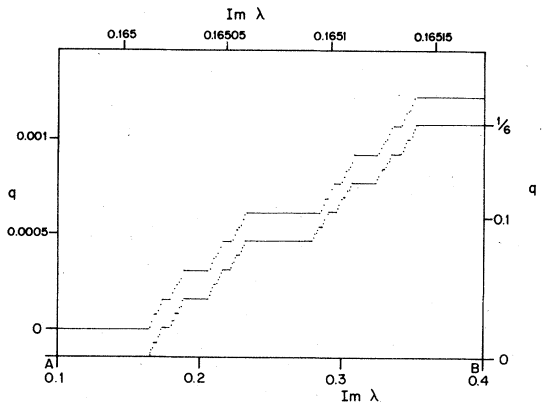

FIG. 9. Variation of wave number across the phase diagram. The lower plots show $q(\lambda)$ along the section AB in Fig. 8, namely $\mathrm{Re}\lambda + \mathrm{Im}\lambda = 0.70$. The upper plot depicts a portion of the lower trace magnified by 1460 times in the horizontal and by 128 times in the vertical directions, respectively, to demonstrate the high degree of self-similarity of this "devil's staircase."

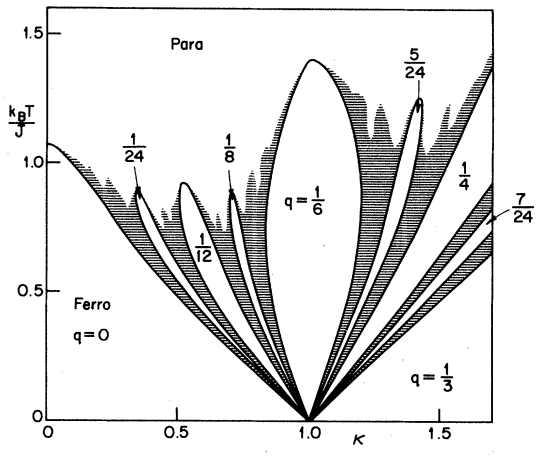

FIG. 10. The same phase diagram for $d = 2.5$ as in Figs. 4 and 8 replotted in the (T, κ) plane to illustrate the analogy with the multiphase behavior of the ANNNI model (Refs. 3 and 5). The locus AB in Fig. 8 and the wave-number plots of Fig. 9 correspond to a locus in this representation running from the Ferro or $q = 0$ phase to the central $q = \frac{1}{6}$ phase, which corresponds to the (3,3) or $\langle 3 \rangle$ phase (Ref. 5) in the ANNNI model.

trace of Fig. 9 with a scale appropriate to demonstrate an apparent high degree of self-similarity of the graph: it looks essentially the same no matter what power of magnification is used to examine it. This self-similarity appears to be strictly true only for $d \geq d_f$. Each "step" in this "devil's staircase"[15] represents an ordered phase. For $d < d_f$ there is actually a "ramp" of finite slope between each pair of adjacent steps where q varies continuously. This ramp represents the region of paramagnetic phase between the two ordered phases. As indicated above, to see the incompleteness of the devil's staircase shown in Fig. 9 requires examining it at scales of order 10^{-9} in $\mathrm{Im}\lambda$. For $d \geq d_f$, however, the phrase "pair of adjacent steps" is meaningless, because between any two steps there are an infinite number of additional steps, just as between any two rational numbers there are an infinite number of additional rational numbers.

In Fig. 10 the phase diagram for $d = 2.50$ exhibited in Fig. 8 is shown replotted in the (T, κ) plane to illustrate its resemblance to phase diagrams of the ANNNI model obtained by other methods.[3–5] The correspondence between $(k_B T/J, \kappa)$ and $\{T_l\}$ is obtained by equating (3.1) and (3.8) and, explicitly, is

$$2J/k_B T = \ln(T_0^2/T_1 T_2) \ , \tag{7.1}$$

$$2\kappa J/k_B T = \ln(T_1/T_2) \ . \tag{7.2}$$

These phase diagrams contain an infinite number of distinct ordered phases and an infinite number of fixed cycles (not illustrated). The principle ordered phases, with the wave number of the modulations in the local order satisfying $q = m2^{-n}/3$ with n small, occupy relatively large areas of the phase diagram. Between these principle phases are regions where there are many ordered phases, each occupying a very slender strip of the phase diagram or else restricted to just a single line. For $d < d_f \simeq 2.625$ there are also strips of paramagnetic phase between all ordered phases. Within these regions of many slender phases the correlation length is always quite large. Thus the whole region is effectively critical and might be regarded as a region of incommensurate algebraic order since a high-resolution experiment or calculation is required to resolve the very slender commensurate phases.

Finally note that our analysis represents the exact solution for the three-state chiral model on the hierarchical pseudolattice described in Sec. V. From that point of view the details of the phase diagrams are of concrete interest. However, the problem of greater physical interest is the model on a hypercubic lattice. The Migdal-Kadanoff renormalization scheme probably generates only a very rough approximation for that problem. Only the coarser, more qualitative features of the phase diagrams we have exhibited should be taken seriously as possibly applying to the three-state chiral model on a hypercubic lattice.

It is worth remarking that even more intricate phase diagrams may be obtained by considering p-state models with $p > 3$ or by adding terms to the Hamiltonian (5.2) which break the cyclic symmetry

of the three-state chiral model. The *full* Hamiltonian space for a general three-state model with spatially isotropic nearest-neighbor interactions only, is eight dimensional. This paper has explored a two-dimensional manifold in that space which is, in a sense, orthogonal to the five-dimensional manifold explored previously in a study of the general three-state model with unbroken exchange symmetry.[21]

ACKNOWLEDGMENTS

I am grateful to Michael E. Fisher, Julia M. Yeomans, and P. Holmes for helpful discussions and, in particular, to Professor Fisher for critical reading of the manuscript. The work has been supported by the National Science Foundation in part through the Materials Science Center at Cornell University.

[1]S. Aubry, in *Solitons in Condensed Matter Physics,* edited by A. R. Bishop and T. Schneider (Springer-Verlag, Berlin, 1978), p. 264.
[2]R. J. Elliott, Phys. Rev. 124, 346 (1961).
[3]W. Selke and M. E. Fisher, Phys. Rev. B 20, 257 (1979); Z. Phys. B 40, 71 (1980).
[4]P. Bak and J. von Boehm, Phys. Rev. B 21, 5297 (1980).
[5]M. E. Fisher and W. Selke, Phys. Rev. Lett. 44, 1502 (1980); Philos. Trans. R. Soc. London (1981) (in press).
[6]J. Villian and M. B. Gordon, J. Phys. C 13, 3117 (1980).
[7]S. Ostlund, Phys. Rev. B 24, 398 (1981).
[8]R. B. Potts, Proc. Cambridge Philos. Soc. 48, 106 (1952).
[9]J. V. José, L. P. Kadanoff, S. Kirkpatrick, and D. R. Nelson, Phys. Rev. B 16, 1217 (1977).
[10]D. R. Nelson and M. E. Fisher, Ann. Phys. (N.Y.) 91, 226 (1975).
[11]A. A. Migdal, Sov. Phys. JETP 42, 743 (1976).
[12]L. P. Kadanoff, Ann. Phys. (N.Y.) 100, 359 (1976).
[13]G. Forgacs and A. Zawadowski (unpublished).
[14]A. N. Berker and S. Ostlund, J. Phys. C 12, 4961 (1979).
[15]B. B. Mandelbrot, *Fractals: Form, Chance, and Dimension* (Freeman, San Francisco, 1977).
[16]Y. Gefen, B. B. Mandelbrot, and A. Aharony, Phys. Rev. Lett. 45, 855 (1980).
[17]J. Stephenson, Can. J. Phys. 48, 1724 (1970).
[18]For simplicity it is assumed that the eigenvectors all exist. This assumption is not necessary for the argument that follows, as is shown by W. J. Camp and M. E. Fisher, Phys. Rev. B 6, 946 (1972).
[19]D. A. Huse, M. E. Fisher, and J. M. Yeomans, Phys. Rev. B 23, 180 (1981); J. Appl. Phys. 52, 2028 (1981).
[20]See, e.g., M. E. Fisher, Rev. Mod. Phys. 46, 597 (1974).
[21]M. Kaufman, R. B. Griffiths, J. M. Yeomans, and M. E. Fisher, Phys. Rev. B 23, 3448 (1981); J. M. Yeomans and M. E. Fisher, Phys. Rev. B 24, 2825 (1981).